An X-Ray Study of Lobe-Dominated Radio-Loud Quasars with XMM-Newton [*]

Li-Ming Dou[1,2] and Wei-Min Yuan[1]

[1] National Astronomical Observatories/Yunnan Observatory, Chinese Academy of Sciences, Kunming 650011, China; *dlm@ynao.ac.cn*
[2] Graduate School of Chinese Academy of Sciences, Beijing 100049, China

Abstract We report on our results of X-ray spectral analysis for a sample of radio-loud quasars covering a wide range of the radio core-dominance parameter, R, from core-dominated to lobe-dominated objects, using data obtained mostly with the XMM-Newton Observatory. We find that the spectral shape of the underlying power-law continuum is flat even for the lobe-dominated objects (average photon index $\sim$ 1.5), indistinguishable from that of core-dominated quasars. For lobe-dominated objects, contribution of X-rays from the jets is expected to be very small based on previous unification schemes, more than one order of magnitude lower than the observed X-ray luminosities. Assuming that radio-loud quasars follow the same X-ray–UV/optical luminosity relation for the disk-corona emission as found for radio-quiet quasars, we estimate the X-ray flux contributed by the disk-corona component from the optical/UV continuum. We find that neither the luminosity, nor the spectral shape, of the disk-corona X-ray emission can account for the bulk of the observed X-ray properties. Thus in lobe-dominated quasars, either the disk-corona X-ray emission is much enhanced in strength and flatter in spectral shape (photon index $\sim$ 1.5) compared to normal radio-quiet quasars, or their jet X-ray emission is much enhanced compared to their weak radio core-jet emission. If the latter is the case, our result may imply that the jet emission in X-rays is less Doppler beamed than that in the radio. As a demonstrating example, we test this hypothesis by using a specific model in which the X-ray jet has a larger opening angle than the radio jet.

Key words: galaxies: active — quasars: general — galaxies: X-ray — galaxies: radio continuum

1 INTRODUCTION

About 15 percent of quasars are classified as radio loud (e.g. Ivezić et al. 2002), based on the strength of the radio emission relative to the optical emission (Kellermann et al. 1989). Radio observations have shown that relativistic jets emanate from quasar nuclear region, and feed approximately symmetric, diffuse radio lobes at a large distance. Radio-loud quasars show diverse radio morphology in observations: core-dominated quasars in which the radio emission comes mostly from the core with flat spectrum, and lobe-dominated quasars in which most of the radio emission comes from the extended region with steep spectrum. The diverse radio morphology is well explained in terms of unification schemes of radio-loud active galactic nuclei (AGN) (Urry & Padovani 1995): the radio emission of quasars is mainly composed of two components, a flat-spectrum, core-jet component which is highly anisotropic due to relativistic Doppler beaming, and a steep-spectrum, extended/diffuse component thought to be mostly isotropic. The appearance of a radio-loud quasar in radio morphology and spectral shape is thus dependent on the inclination angle of the

jet axis to the observer. At a small inclination angle, the core-jet emission can be tremendously Doppler boosted due to strong beaming effects, and outshines the extended emission. In this case we see a core-dominated quasar. Moreover, at a large inclination angle the observed core-jet emission is largely depressed and generally much weaker than the isotropic radio lobe emission, as such a lobe-dominated quasar is observed. In observations, radio core-dominance, defined as the radio flux ratio of the core to the extended emission ($R \equiv F_{\rm core}/F_{\rm ext}$, Orr & Browne 1982), normally at 5 GHz, is used as an indication of jet inclination angle, which itself is difficult to measure. Core-dominated sources, seen at small angles, have large core-dominance parameters, and vice versa. In this line, unification models of radio-loud quasars have been widely investigated in the literature (see Urry & Padovani 1995 for a review).

Radio-loud quasars are strong X-ray emitters. Tananbaum (1983) and subsequent studies found that the X-ray flux is correlated with the radio core flux. The correlation is particularly strong among core-dominated objects. For example, based on a large sample of quasars detected with ROSAT, Brinkmann et al. (1997) found a nearly linear relation between the X-ray and radio core fluxes for extremely core-dominated objects ($R > 10$). The close link with radio core-jet emission suggested that the X-ray emission originates from the jet, too (Ghisellini et al. 1993). Assuming that the core radio flux traces the jet X-ray flux, independent of jet orientation, it was found that the jet to the total X-ray luminosity ratio increases with R for lobe-dominated objects, while it becomes independent of R for core-dominated objects (Kembhavi 1993; Brinkmann et al. 1997). This means that the X-ray emission is dependent on radio core-dominance, i.e., on the orientation of the jet to the observer. A recent study by Landt et al. (2006) yielded similar results. It has also been found that core-dominated (flat-spectrum) quasars have flatter X-ray spectra than lobe-dominated (steep-spectrum) quasars (Brinkmann et al. 1997).

To explain observations as mentioned above, phenomenological models on X-ray emission within the framework of unification schemes have been suggested (Kembhavi 1986, 1993; Browne & Murphy 1987; Baker et al. 1995; Siebert et al. 1998; Brinkmann et al. 1997). In these scenarios, the observed X-rays originate from at least two components, one rather anisotropic component from relativistic jets, and the other supposedly much less anisotropic emission with a possibly steep X-ray spectrum. The X-ray emission from relativistic jets has flat X-ray spectra (Williams et al. 1992; Lawson & Turner 1997; Reeves & Turner 2000). In commonly accepted radiation models, this emission is produced by high-energy electrons in relativistic jets via the inverse Compton (IC) process. Based on the origins of seed photons, the IC process can be either synchrotron self-Compton (SSC), where seed photons are from jet synchrotron emission itself, or external Compton (EC), where seed photons come from infrared emission of the accretion disk (Ghisellini 1993).

Recent X-ray observations by Chandra, with its superb spatial resolution, confirmed that the bulk of the X-ray emission from radio-loud quasars remains mostly unresolved and is associated with the compact radio core (Gambill et al. 2003). Although X-rays from resolved large-scale jets (hot spots, knots) and lobes have been detected (Brunetti et al. 2002; Siemiginowska et al. 2003; Kataoka & Stawarz 2005; Kraft et al. 2007), they constitute only a very small portion of the total observed X-ray flux (Brunetti et al. 2001; Isobe et al. 2002, 2005; Hardcastle et al. 2002; Yuan et al. 2003; Kataoka et al. 2003, 2005). Direct detection of large-scale X-ray jets also supports the above jet X-ray emission scenario. In addition, other possible contributions to the X-ray emission from nuclear region in radio-loud quasars are X-rays emitted from the accretion disk and its hot corona, as observed in radio-quiet quasars. They include a power-law type continuum up to several tens of keV with a steep index ($\Gamma \sim 1.9$ or 2.0, Piconcelli et al. 2005; Reeves & Turner 2000; Feiore et al. 1998; Nandra et al. 1997a,b, Shastri 1991; Wilkes & Elvis 1987), sometimes accompanied by (broadened) Fe Kα lines (Jiménez-Bailón et al. 2005; Gliozzi et al. 2003), and, in some cases, a steep soft X-ray excess component (Brinkmann et al. 1998; Yuan et al. 2000).

Despite the success of unification schemes in explaining the X-ray emission components of radio-loud quasars, questions remain unanswered as to the nature of the less anisotropic X-ray component. In Brinkmann et al. (1997) this component is postulated as the disk-corona X-ray emission as seen in radio-quiet quasars. Moreover, a potential uncertainty is that previous unification models were based mostly on X-ray data in the soft band (e.g. in the 0.1–2.4 keV ROSAT band), and therefore further testing using data in a broad (hard) X-ray band is required. This has become possible with the advent of the most advanced, relatively broad band X-ray satellites XMM-Newton and Chandra (up to 10 keV) currently in operation. Although there are articles in the literature on the X-ray properties of individual or small sample of radio-loud quasars (Gambill et al. 2003; Piconcelli et al. 2005; Belsole et al. 2006), there has been so far no

devoted study especially focusing on the orientation dependent X-ray properties in terms of unification schemes. In this paper, we present a study in line with this idea. We make use of the X-ray data, obtained mainly with XMM-Newton, for a small sample of radio-loud quasars, which covers a wide range of radio core-dominance parameters, R. We find that, considering their very weak radio core fluxes, lobe-dominated quasars show much enhanced, flat-spectrum X-ray emission, which cannot be accounted for by X-rays from the black hole accretion process. The result is at odds with the commonly accepted simple unification schemes. We also give possible explanation to the results. We describe the sample and X-ray data in Section 2. In Section 3 the X-ray data analysis is described for the objects in the sample, some of which are presented for the first time. The results are given in Section 4, and their implications are discussed in Section 5, followed by a summary in Section 6. Throughout the paper, a set of cosmological parameters in which $H_0 = 70\,\mathrm{km\,s^{-1}\,Mpc^{-1}}$, $\Lambda = 0.7$ and $\Omega_m = 0.3$, is assumed. Errors in X-ray spectral fitting are quoted at the 90% confidence level (for each parameter).

2 THE SAMPLE AND THE X-RAY DATA

The quasars are selected from the large radio-loud X-ray quasar sample of Brinkmann et al. (1997), which was based on the catalog of Veron-Cetty & Veron (1993). We mainly use XMM-Newton (Jansen et al. 2001) data in this study, simply because, compared to Chandra, XMM-Newton has detected a much larger number of serendipitous objects, thanks to its large field of view ($\sim$30 arcmin in diameter). We match its sub-sample which has core-dominance parameters measured with the XMM-Newton database [1]. To enable reliable spectral analysis, we select only objects with good spectral signal-to-noise ratios and with the summed net source counts more than 2000 for the three XMM-Newton EPIC cameras. This results in a total of 12 objects with both R parameters and good XMM spectra available. Among these, there are five core-dominated quasars ($R > 1.0$) and seven lobe-dominated quasars ($R < 1.0$). Albeit small, our sample spans a wide range of R, from core-dominated ($R = 63$) to extremely lobe-dominated objects ($R = 0.01$). A large R range is essential for testing orientation dependent X-ray emission and unification schemes. In order to find out possible trends with the change of R, we further split the lobe-dominated quasars into two groups, i.e. mildly lobe-dominated ($0.5 < R < 1.0$) and lobe-dominated ($R < 0.5$) objects. Our sample objects are all typical, powerful quasars with strong, broad optical/UV emission lines. The core-dominated (flat-spectrum) quasars are typical blazars (Brinkmann et al. 1997), showing compact radio morphology. Given their high radio power at low frequency above the FR I/FR II dividing value ($\sim 2 \times 10^{25}\,\mathrm{W\,Hz^{-1}\,sr^{-1}}$, Fanaroff & Riley 1974), our lobe-dominated radio sources are all of the FR II type, as is common for powerful radio quasars.

Table 1 lists the sample objects, their 5 GHz radio core fluxes, radio core-dominance, and the relevant information on the X-ray observations. The radio data and the radio core dominance parameters are taken from Brinkmann et al. (1997), except 4C 06.41 for which the radio core dominance is 2.13 at 15 GHz from VLBA observation (Kovalev et al. 2005). For the relatively well-studied lobe-dominated quasar, 3C 249.1, the data are taken as a target in our own XMM-Newton proposal. For this object, observations with Chandra and ASCA are also available, and are also used in this study. Our sample includes three objects (PG 0007+106, 3C249.1 and B2 1512+37) for which XMM data have been published in a previous X-ray study of the PG quasar sample (Piconcelli et al. 2005).

For all the objects in our sample, the XMM-Newton Observation Data Files (ODFs) were retrieved from the XMM Science Archive[2], and reprocessed using the SAS (Science Analysis System) version 6.5 (Loiseau et al. 2005) with the most recent calibration files. The events files for the PN, MOS1 and MOS2 cameras are produced by the *epchain* and *emchain* tools, respectively. Only events flagged as PATTERN≤4 for PN and ≤12 for MOS are used for conservative events extraction. Dead pixels, hot pixels and high background flaring periods have been removed. Source X-ray counts are extracted within a circle of a radius corresponding to more than 80% enclosed energy of the PSF. The local background is extracted from source free regions, whenever possible, in the way as suggested in the XMM-Newton data analysis manual as appropriate, i.e. for PN, a circle at the same CCD readout columns and an annulus around the source for MOS1 and MOS2. The response and ancillary files are created with the RMFGEN and ARFGEN tools

---

[1] We used the 2XMMp catalogue, released on 2006 July 24, "The Second XMM-Newton Serendipitous Source Pre-release Catalogue, XMM-Newton Survey Science Centre, 2006".

[2] see *http://xmm.vilspa.esa.es*.

Table 1 The Sample and Information on X-ray Observations

Name	Obs. Id	Obs.date	Instrument	Frame	Filter	time	z	Gal.N_H	flux$_{core}$	R
B2 0937+39	0203270101	2004–05–17	pn,mos1,mos2	Full	Medium	36.1	0.617	1.5[a]	0.005	0.015
3C 249.1	74050000	1996–03–12	ASCA(SIS,GIS)	-	-	36.6				
3C 249.1	0153210101	2002–11–01	pn,mos1,mos2	Full	Medium	5.8	0.312	2.73[b]	0.108	0.123
3C 249.1	03986	2003–07–02	Chandra(ACIS)	-	-	24.0				
B2 1512+37	0111291001	2002–08–25	pn,mos1,mos2	Large	THIN1	17.6	0.371	1.36[c]	0.068	0.195
4C 19.31	0101440401	2000–11–07	pn	Full	Medium	37.5	1.691	3.12[a]	0.058	0.269
MARK 992	0201090401	2004–01–23	pn,mos1,mos2	Full	THIN1	14.3	0.654	5.53[a]	0.082	0.53
PKS 0405–12	0202210401	2005–02–04	pn,mos1,mos2	Large,Full	THIN1	61.2	0.573	3.81[a]	0.96	0.59
3C 207.0	0147670301	2003–10–16	pn,mos1,mos2	Full	Medium	4.4	0.681	4.12[a]	0.657	0.61
4C 06.41	0151390101	2003–05–18	pn,mos1,mos2	Full	THIN1	40.3	1.27	2.85[a]	1.40	2.13
PKS 1302–102	0032141201	2002–01–03	pn,mos1,mos2	Full	Medium	11.5	0.278	3.33[a]	1.02	3.09
PG 0007+106	0127110201	2000–07–03	pn,mos1,mos2	Small,Timing	THIN1	9.9	0.089	6.09[d]	0.151	27.54
B2 1308+32	0020540401	2002–12–10	mos2	Full	THIN1	48.6	0.996	1.10[a]	1.574	50.1
PKS 1502+106	0205340401	2005–07–17	mos1,mos2	Timing,Small	THIN1	20.9	1.839	2.36[a]	2.516	63.1

Col.(1): quasar name; Col.(2): observation ID; Col.(3): observation date; Col.(4): telescope instrument; Col.(5): Frame; Col.(6): Filter; Col.(7): good exposure time (ks) of the first instrument; Col.(8): redshift; Col.(9): Galactic column density N_H (10^{20} cm^{-2}); Col.(10): 5-GHz flux density of radio core (Jy); Col.(11): radio core-dominance. Reference for Galactic N_H values: [a] Dickey & Lockman (1990), [b] Kalberla et al. (2005), [c] Stark et al. (1992), [d] Elvis et al. (1989).

of the SAS software, respectively, using the latest calibration files (see Loiseau et al. 2005). The Chandra data of 3C249.1 is reprocessed following the standard algorithm using CIAO v3.2 with the CALDB v3.2.4 calibration database[3]. The source counts are extracted from a circle of radius 8 arcsec to include more of the extended emission in this object and background counts from a circle of radius 15 arcsec near the source. We examine any possible pile-up effect in our observations by using the SAS tool *epatplot*, and find that it is insignificant in all of the observations (both PN and MOS).

All the extracted spectra are rebinned as default binning factors, and are grouped in such a way that there are a minimum of 25 counts in each bin. We use the XSPEC version (12.2.1) for spectral fitting. Given the very similar response matrices and effective area files for MOS1 and MOS2, and the fact that the two MOS spectra agree well with each other, they are co-added to form a single spectrum (using the FTOOL *addspec* software). The same is true for the two SIS and two GIS spectra for the ASCA data for 3C249.1.

3 X-RAY SPECTRAL ANALYSIS

In our spectral analysis, we first fit the co-added MOS1/2 and PN spectra respectively and compare their results. We find that for all of our objects the MOS and the PN spectra agree well with each other within the mutual statistical uncertainties. Therefore, we fit jointly the MOS and the PN spectra for each object by tying the parameters of models except the normalization constants for the MOS and PN. We report the results of spectral fitting obtained in this way only for their improved statistical uncertainties.

We first fit the spectra with a simple power law with absorption fixed at the Galactic column density. Among the sample, only two objects, PKS 1502+106 and B2 1308+32, both core-dominated, can be fitted with such a model. For most of the remaining objects, the fits result in large residuals in the soft X-ray band, indicative of the presence of an excess component. For them, at least two-component models are used. We then model their spectra with a power-law for the underlying continuum dominating the hard X-ray band, and a steep component contributing to the soft X-ray band. We find that using a power-law for the steep component gives the best and acceptable fits for all except two objects. For one of these two objects, 4C 19.31, a blackbody gives the similar fit as a power-law for the soft component; while for the other, PKS 0405–12, the soft excess component is best fitted with a power law plus a blackbody. X-ray absorption in excess of the Galactic value is found in one object: 3C 207.0, a mildly lobe-dominated source. The detailed results of spectral fitting are given below for each object individually, and the fitted key parameters are summarized in Table 2. We also show, as examples, other spectra and the best-fit models for some of the objects, which are chosen to represent the class of objects and/or the class of models.

---

[3] *http://cxc.harvard.edu/ciao/guides*

Table 2 Results of Spectral Fitting

Name	model	Γ_1	Norm1	Γ_2	Norm2	nH/T	χ^2/d.o.f
B2 0937+39	2p	$1.59^{+0.03}_{-0.03}$	0.9	$3.09^{+0.10}_{-0.09}$	0.3	-	236/236
3C 249.1			3.7		1.6		
3C 249.1	$2p^a$	1.6(f)	5.7	$2.41^{+0.10}_{-0.10}$	4.7	-	636/599
3C 249.1			1.8		3.3		
B2 1512+37	$2p^b$	$1.51^{+0.09}_{-0.09}$	5.0	$2.71^{+0.22}_{-0.15}$	9.0	-	226/253
4C 19.31	2p	$1.44^{+0.10}_{-0.10}$	0.5	$2.71^{+0.24}_{-0.22}$	0.4	-	67/60
MARK 992	2p	$1.23^{+0.09}_{-0.08}$	0.6	$2.41^{+0.05}_{-0.05}$	1.7	-	139/127
PKS 0405-12	$2p+bb^c$	$1.50^{+0.05}_{-0.06}$	7.7	$2.96^{+0.09}_{-0.08}$	6.9	$-/0.57^{+0.09}_{-0.09}$	192/169
3C 207.0	abs+po	$1.78^{+0.05}_{-0.05}$	4.4	-	-	$16.5^{+2.8}_{-2.6}$	273/249
4C 06.41	2p	1.46	0.25	$2.61^{+0.07}_{-0.11}$	0.41	-	176/190
PKS 1302-102	2p	$1.23^{+0.05}_{-0.05}$	2.7	$2.54^{+0.04}_{-0.04}$	6.3	-	217/197
PG 0007+106	p+bb	$1.70^{+0.02}_{-0.04}$	16.5	-	-	$-/0.18^{+0.02}_{-0.02}$	509/529
B2 1308+32	p	$1.60^{+0.02}_{-0.02}$	7.5	-	-	-	85.67/91
PKS 1502+106	p	$1.62^{+0.07}_{-0.07}$	1.1	-	-	-	56.25/61

Col.(1): quasar name; Col.(2): the best fit model (p: one power-law; 2p: two power-laws; abs+po: absorption power-law; p+bb: one power-law and a blackbody 2p+bb: two power-laws and a blackbody); Col.(3): photon index of the underlying continuum; Col.(4): normalization of the underlying continuum (10^{-4} photons keV^{-1} cm^{-2} s^{-1}); Col.(5): the steep power-law component photon index; Col.(6): normalization of the steep power-law component (10^{-4} photons keV^{-1} cm^{-2} s^{-1}); Col.(7): intrinsic neutral hydrogen column density (10^{20} cm^{-2}), or the blackbody component temperature (keV). Col.(8): χ^2 and degrees of freedom.
a: We fit the three spectra together, and fix the flat power law component photon index at 1.6 (see text for details).
b: The fitting results are taken from Piconcelli et al. (2005).
c: Two absorption edges are needed at $2.61^{+0.06}_{-0.06}$ keV and $8.49^{+0.16}_{-0.15}$ keV.

3.1 Core-Dominated Quasars ($R > 1.0$)

3.1.1 4C 06.41

The radio core-dominance of 4C 06.41 is 2.13 at 15 GHz from observations with the VLBA (Kovalev et al. 2005). A noticeable sharp absorption feature is present at ~ 1.8 keV in the spectrum. Since there is neither absorption edge nor line known close to the corresponding energy in the source rest frame (E~ 4.1 keV), and since the feature has exactly the same energy as the sharp drop of the effective area due to the instrumental absorption edge, we attribute this feature to the imperfectness of the calibration, which is sometimes seen in XMM-Newton EPIC spectra at around 1.8 keV (see Kirsh et al. 2007, see also the XMM calibration web-page [4]). We therefore omit data within 1.7–2.0 keV in the fit. We first fit the spectrum in the 2–10 keV range with a power-law with fixed Galactic absorption column density, which yields a power-law photon index $\Gamma = 1.46$. We then extend the spectral fit down to low energies. A substantial soft X-ray excess is present above the extrapolation. Then we fit the spectra using two-component models, with the photon index of the underlying power-law fixed at $\Gamma = 1.46$. We find that the best-fit for the soft X-ray excess is a power law, with $\Gamma = 2.61^{+0.07}_{-0.11}$. The spectra and the best-fit model are shown in Figure 1 as a demonstration.

3.1.2 PKS 1302–102

The best-fit model has two power-law components (χ^2/d.o.f = 217/197) with $\Gamma_1 = 1.23^{+0.05}_{-0.05}$ and $\Gamma_2 = 2.54^{+0.04}_{-0.04}$, respectively.

3.1.3 PG 0007+106

Strictly speaking, this object may not be a truly radio-loud quasar owing to its weak radio jet emission. It is sometimes classified as a radio-intermediate or even radio-quiet quasar based on the radio-to-optical flux ratio definition. It is classified as a core-dominated quasar based simply on its radio morphology. In fact, it is one of the radio-intermediate objects where Doppler effect boosts radio emission from a relativistic jet (Falcke et al. 1996; Lister & Homan 2005). The XMM-Newton-spectrum of this object has been previously studied by Salvi et al. (2002) and Piconcelli et al. (2005). The best-fitted model reported in Piconcelli et al. (2005) is a power-law ($\Gamma=1.71^{+0.04}_{-0.04}$) with a blackbody component ($T = 0.16^{+0.01}_{-0.01}$ keV) and an Fe Kα line

---

[4] *http://xmm.vilspa.esa.es/es/external/xmm_sw_cal/calib/index.shtml*
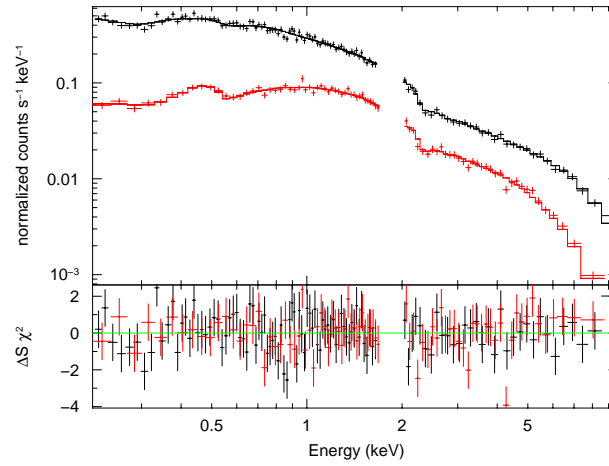
Fig. 1 XMM-Newton spectra of 4C 06.41 (top panel). The upper and lower spectra correspond to the PN and MOS data, the best-fit model is depicted by the solid curves. The bottom panel shows residuals as contribution to χ^2.

($EW = 220^{+110}_{-100}$ eV, Jiménez-Bailón et al. 2005); whereas a simple power law and a very broad Fe Kα line ($EW = 1.25^{+0.31}_{-0.35}$ keV) was claimed by Salvi et al. (2002). We repeat the spectral fitting for this object and find that, indeed, both the above two models yield acceptable fit, though the former is preferred given its better χ^2. Obvious flux variations were found in the radio, infrared, optical, ultraviolet and X-ray bands (Salvi et al. 2002; Teräsranta et al. 2005).

3.1.4 B2 1308+32 and PKS 1502+106

B2 1308+32 and PKS 1502+106 are both core-dominated sources. The best-fit models are a simple power-law with Galactic absorption with $\Gamma = 1.60^{+0.02}_{-0.02}$ and $\Gamma = 1.62^{+0.07}_{-0.07}$ for B2 1308+32 and PKS 1502+106, respectively.

## 3.2 Lobe-Dominated Quasars ($R < 1.0$)

3.2.1 MARK 992

The best-fit model is a two power-law model (χ^2/d.o.f=139/127). The power-law indices are $\Gamma_1 = 1.23^{+0.09}_{-0.08}$ and $\Gamma_2 = 2.96^{+0.09}_{-0.08}$, respectively.

3.2.2 PKS 0405–12

The best-fit model is a power-law with a soft excess, which is described with another steep power-law plus a blackbody. Two absorption edges are marginally detected at $2.61^{+0.06}_{-0.05}$ keV and $8.49^{+0.16}_{-0.15}$ keV, respectively, which may arise from the absorption edges of H-like Si and Fe XXIII and Fe XXIV ions, respectively. The spectra and the best-fit model are shown in Figure 2.

3.2.3 3C 207.0

The best-fit model is a single absorbed power-law ($\Gamma = 1.77^{+0.05}_{-0.05}$) with neutral absorption (χ^2/d.o.f = 273/249). Excess absorption is required ($N_{\rm H} = 1.65^{+0.28}_{-0.26} \times 10^{21}$ cm^{-2}) for an intrinsic absorber, confirming the results based on Chandra data (Brunetti et al. 2002). Brunetti et al. (2002) also found that while the vast majority of the X-ray emission comes from the nucleus, there exists extended emission from hot spots and knots, and radio lobes. Compared to the Chandra spectrum ($\Gamma = 1.22^{+0.06}_{-0.05}$), the XMM-Newton spectrum is steeper, and also shows a flux higher by a factor of 2.7 at 1 keV. The spectra and the best-fit model are shown in Figure 3.
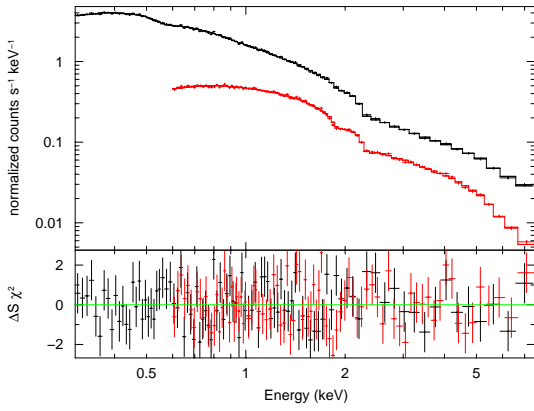
Fig. 2 Spectra of PKS 0405-12 and the best-fit model (the symbols are the same as in Fig. 1).
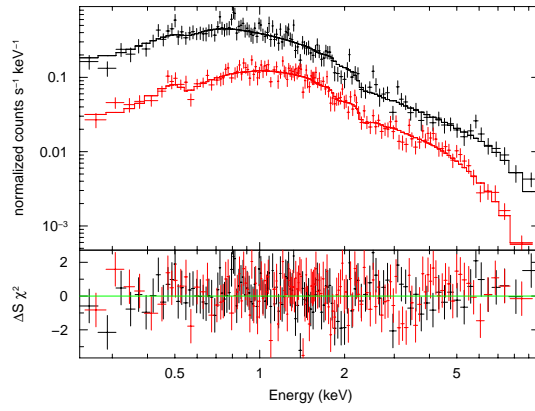
**Fig. 3** Spectra of 3C 207 and the best-fit model (the symbols are the same as in Fig. 1).
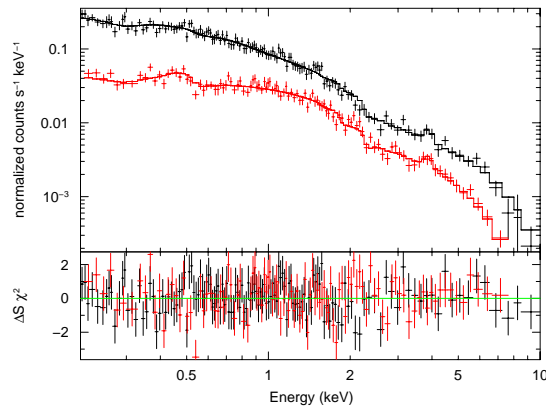
Fig. 4 Spectra of B2 0937+39 and the best-fit model (the symbols are the same as in Fig. 1).

3.2.4 B2 0937+39

B2 0937+39 is the most lobe-dominated quasar ($R = 0.015$) at a redshift of $z = 0.616$. The best-fit model is a flat power-law ($\Gamma = 1.59^{+0.03}_{-0.03}$) with a soft excess component, which is best described with a steep power-law (χ^2/d.o.f =236/236). Using blackbody or bremsstrahlung for the soft X-ray component yields worse χ^2 and somewhat steeper Γ ($\sim 1.7 - 1.8$). An emission line is marginally detected at $6.27^{+0.14}_{-0.16}$ keV in rest frame ($\sigma \sim 0.15$ keV), which may be due to an Fe Kα emission. Adding line reduces χ^2 by 10, corresponding to the 98% confidence using the F-test. The spectra and the best-fit model are shown in Figure 4.

3.2.5 3C 249.1

3C 249.1 is a lobe-dominated quasar. It was observed with ASCA (1996), XMM-Newton (2002, our own proposal), and Chandra (2003). The spectral data are first fitted independently. A simple power-law with Galactic absorption, plus a conspicuous absorption edge at 7.5 keV gives an acceptable fit, yielding a power-law index of 1.77 for the ASCA data. However, for the other two data sets, a soft X-ray excess is required in the fits, which can best be represented by a steep power-law. The underlying continuum is flat, with $\Gamma = 1.58 \pm 0.09$ for the XMM-Newton and $\Gamma = 1.67 \pm 0.17$ for the Chandra spectrum. The absence of the soft X-ray excess in the ASCA spectrum could be due to the relatively higher low-energy cutoff and the
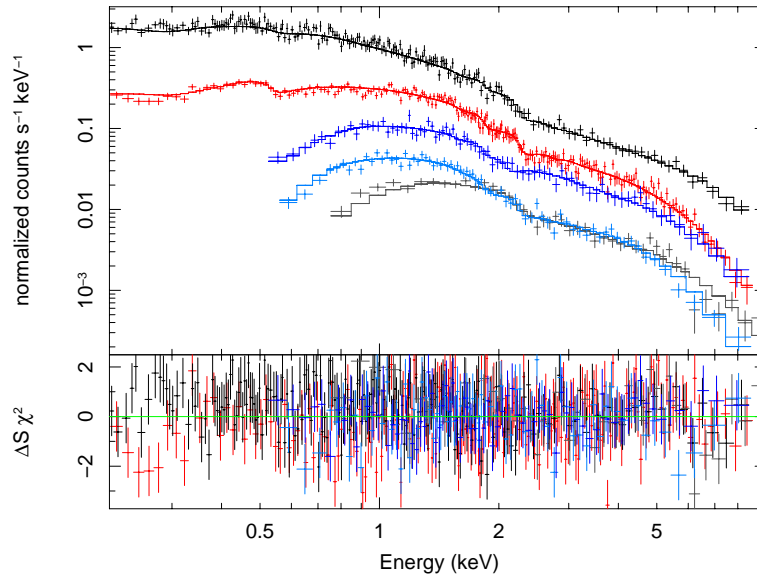
Fig. 5 Spectra of 3C 249.1 (the top panel). From top to bottom each spectrum corresponds to the PN, MOS, ACIS and ASCA(SIS, GIS) data, respecively. The best-fit model is represented by the solid curves. The bottom panel shows the residuals as contribution to χ^2.

low efficiency in the soft X-ray band of ASCA. Assuming the same spectral models, the spectra from the three different missions are fitted jointly; in doing so the photon index Γ_1 for the underlying continuum is fixed at $\Gamma = 1.6$ and Γ_2 for the soft excess component is tied together for the three data sets. The model can fit the spectra of the three data sets well. The spectra and the best-fit model are shown in Figure 5. Flux variations between these observations, mostly in the soft X-ray excess component, are also found. What is puzzling is the absorption edge, arising probably due to the Fe K-shell absorption which disappears in both the XMM-Newton and the Chandra spectra.

3.2.6 B2 1512+37

The best-fit model is a two power-law model (χ^2/d.o.f =226/253), in which one is a flat component with $\Gamma = 1.51^{+0.09}_{-0.09}$ and the other is a steep compoent with $\Gamma = 2.71^{+0.22}_{-0.15}$. The results are taken from Piconcelli et al. (2005). A Chandra observation revealed that there is extended X-ray emission from the lobes, but much fainter compared to the emission from core (Stockton et al. 2006). For this object, polarization in the infrared, optical, and radio bands were also observed (Sitko & Zhu 1991; Hutsemékers et al. 2005; Haves et al. 1974).

3.2.7 4C 19.31

The best-fit model is a two power-law model (χ^2/d.o.f=67/60) with photon indices of $\Gamma_1 = 1.44^{+0.10}_{-0.10}$ and $\Gamma_2 = 2.71^{+0.21}_{-0.15}$, respectively.

3.3 Summary of Spectral Analysis Results

We find that most of the objects in our sample, regardless of their core-dominance parameters, show a ubiquitous flat power-law as the underlying continuum plus a steep component is dominating the soft X-ray band. The most interesting result is the flat power-law continuum found in lobe-dominated quasars. The photon indices are all around $\Gamma \sim 1.5$ (from 1.44 to 1.60), indistinguishable between core-dominated and lobe-dominated quasars. The flat power-law continuum in lobe-dominated quasars has also been found by Belsole et al. (2006).

Table 3 Luminosities of the Objects in our Sample

Name	$\log(L_{5\,\mathrm{G}}^{\mathrm{core}})$	$\log(L_{2500})$	$\log(L_{2\,\mathrm{keV}})$
B2 0937+39	31.69	30.46	26.9
3C 249.1	32.37	30.74	27.3
B2 1512+37	32.41	30.84	27.1
4C 19.31	33.61	31.41	27.9
MARK 992	32.95	30.80	27.2
PKS 0405–12	33.91	31.59	27.8
3C 207.0	33.89	30.37	27.6
4C 06.41	34.76	31.55	28.2
PKS 1302–102	33.28	30.98	26.8
PG 0007+106	31.43	30.07	26.2
B2 1308+32	34.61	31.86	28.3
PKS 1502+106	35.31	30.98	28.2

Col.(1): the quasar name; Col.(2): logarithmic monochromatic luminosity of radio core at 5 GHz (erg s^{-1} Hz^{-1}); Col.(3): logarithmic monochromatic optical luminosity at 2500 Å calculated from the $B-$band magnitude (erg s^{-1} Hz^{-1}); Col.(4): logarithmic monochromatic X-ray luminosity at 2 keV (erg s^{-1} Hz^{-1}).

In addition, some interesting features are found for a few objects. PG 0007+106, which is known to have a weak radio jet, is found to show a 'soft X-ray excess' and an Fe Kα line at 6.4 keV. It is thus expected that its X-rays are dominated by the disk-corona emission. An Fe Kα line is also possibly found in the lobe-dominated object B2 0937+39. Excess X-ray absorption is found in the lobe-dominated quasar 3C 207.0.

We list the 2 keV X-ray luminosities in Table 3, as well as the radio core luminosities at 5 GHz, and the optical luminosities at 2500 Å. X-ray luminosities are corrected for all the relevant absorption.

4 ORIENTATION DEPENDENT X-RAY EMISSION

Following Brinkmann, Yuan & Siebert (1997), we plot in Figure 6 the unabsorbed 2 keV X-ray luminosity versus the 5 GHz radio core luminosity for the objects in our sample. We also mark the data taken in three observations of 3C249.1, which show flux variations. As can be seen there is a weak dependence of the X-ray luminosity on the radio core luminosity. The Spearman correlation test yields a probability of no correlation of $P \sim 0.03\%$, and a slope of ~ 0.5 is obtained when performing a simple regression analysis. In fact, the result is similar to what was found previously, though the sample is small. Using only extremely core-dominated quasars ($R > 10$), Brinkmann et al. (1997, see their fig. 15) found a close and nearly linear relation between the X-ray and radio core fluxes,

$$\log L_{\mathrm{x}} = 0.97(\log L_{\mathrm{rc}} - 34) + 27.17, \tag{1}$$

where L_{rc} is the core-jet radio luminosity at 5 GHz, and L_{x} the X-ray luminosity at 2 keV. This correlation suggests that the X-ray emission is dominated by X-rays from the jet in these objects, which can be traced by L_{rc} via Equation (1) (Brinkmann et al. 1997). Following the commonly accepted unification schemes, we assume that the jet X-ray and radio core flux relation given in Equation (1) can be extrapolated to low L_{rc} and is valid for all radio-loud quasars of regardless of their core-dominance parameters. In this way, we can estimate the jet X-ray luminosities from radio core luminosities, as represented by the solid line in Figure 6, along with its offsets arising from the 1-σ uncertainties of the parameters (dotted lines).

As can be seen from Figure 6, our core-dominated quasars generally follow the $L_{\mathrm{x}} \sim L_{\mathrm{rc}}$ relation, except PG 0007+106 for which the X-ray emission is largely dominated by disk-corona emission. However, all the lobe-dominated quasars show a significant amount of X-ray fluxes in excess of the predicted jet emission. The deviation increases with decreasing radio core luminosities and R. This confirms previous results, in which this 'excess' X-ray component (the second component in unification models), assumed to be less anisotropic or even roughly isotropic, was previously thought to be due to disk-corona X-ray emission, as seen in radio-quiet quasars (Brinkmann et al. 1997).
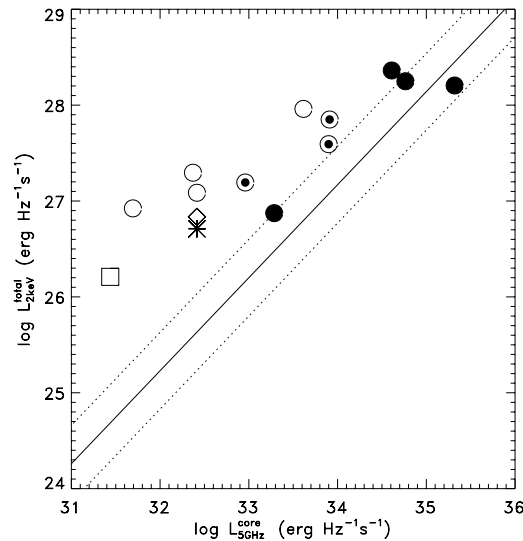
Fig. 6 Relation between the observed (total) X-ray luminosity at 2 keV and the 5 GHz radio core luminosity for the lobe-dominated quasars ($\circ$, radio core-dominance $R < 0.5$), mildly lobe-dominated objects ($\odot$, $0.5 < R < 1.0$), and core-dominated objects ($\bullet$, $R > 1.0$), including PG 0007+106($\square$), and 3C 249.1 ($*$ Chandra data and $\diamond$ ASCA data). The relation between X-ray and radio luminosity arising from core-jet emission as given in Eq. (1), adopted from Brinkmann et al. (1997), is indicated by the solid line, and its $1 - \sigma$ offsets are represented by the dotted lines.

5 DISCUSSION

Summarizing the above analysis, we can draw the following conclusions: (1) The underlying X-ray power-law continuum is flat for almost all the objects, regardless of their radio core-dominance parameters. (2) The X-ray emission of radio-loud quasars is dependent on radio core-dominance. In core-dominated objects the X-ray emission is dominated by jet emission which is predicted by the simple $L_\mathrm{x} \sim L_\mathrm{rc}$ relation, but with the decrease of radio core-jet power, an additional X-ray component rises to dominate the X-rays in lobe-dominated objects. (3) The overall X-ray spectral shape of such an additional component is flat, indistinguishable from core-dominated objects.

Given that the spatial resolution of XMM-Newton is only about 5 arcsec, the observed X-rays may be contributed by X-rays from large scale structures, such as jets (knots or hot spots) or lobes, if present. However, such extended, large scale X-ray emission is, in general, much weaker compared to the core X-ray emission in radio-loud quasars (Gambill et al. 2003). In particular, there are Chandra imaging observations for three of our objects, namely, 3C249.1, B2 1512+37, and 3C 207.0. Results of spatial analysis on these objects, as presented in the literature, revealed that the X-ray emission comes predominately from the compact core (less than only a few kpc), and large-scale structures contribute only a negligible fraction of the observed X-rays (less than 10%, Brunetti et al. 2002; Stockton et al. 2006). We thus argue that extended X-rays from large-scale structures, if any, are too weak to explain the observed enhanced X-ray emission in the lobe-dominated quasars.

In addition to the core origin of the X-ray emission, two more facts should be considered here. The X-ray spectra are most likely flat, comparable to that of jet emission. Secondly, as shown in Figure 8, its luminosity appears to be correlated with the radio core-jet power.

5.1 Contribution from Disk-Corona X-Ray Emission

A part of the X-ray emission of quasars comes from the hot corona of a putative accretion disk, produced by inverse-Compton scattering as disk optical photons collide with energetic corona electrons. This process is believed to be operating in most luminous AGNs and is responsible for the X-ray emission seen in Seyfert

galaxies and radio-quiet quasars. Hereafter we refer to this X-ray emission as the disk-corona component, which has a canonical photon index $\Gamma \approx 2.0$. For radio-quiet quasars, the strength of this X-ray emission is found to be well correlated with the UV/optical continuum emission (such as 2500 Å luminosity as commonly used, e.g. Yuan et al. 1998; Shen et al. 2006). Therefore, it can be estimated from the 2500 Å luminosity of a quasar. Though there is a considerably large scatter for individual objects, the result should be meaningful in the statistical sense for a sample. The problem is that such a relation is not available for radio-loud quasars, because it is usually difficult to disentangle X-rays from disk-corona and from jets. Though the situation is far from being clear as to whether the interplay of accretion disk and corona in radiating in the two bands (UV/optical for the former and X-ray for the latter) is similar in radio-loud and radio-quiet quasars, there is no evidence found against their similarity. Here we assume that radio-loud quasars follow the same disk-corona optical-X-ray luminosity relation as radio-quiet objects. Then the strength of disk/corona X-ray emission can be estimated from the optical luminosity, which are computed from their B-band magnitudes, for the objects in our sample. In this paper, we use the most recent relations given by Shen et al. (2006) found for radio-quiet quasars,

$$\log L_{2\,\mathrm{keV}} = 0.57^{+0.02}_{-0.03}(\log L_{2500} - 30.5) + 0.57^{+0.16}_{-0.12} \log(\frac{1+z}{1.5}) + 26.44^{+0.02}_{-0.02}, \tag{2}$$

where L_{2500} is the luminosity at 2500 Å.

In Figure 7, we plot the estimated 2 keV luminosity ratios of the disk-corona X-ray component to the observed X-rays versus the observed X-ray luminosity. This ratio is an indicator of the relative contribution of the disk-corona emission to the total X-ray luminosity. Figure 7 shows that, for most of the objects, this component makes up from several percent to at most several tens per cent of the total X-ray luminosity. For objects with high X-ray luminosities, this fraction is small, at a level of around 10% (represented by the solid line), which can be understood as the high X-ray luminosities are mainly contributed by jet emission, with large enhancement factors due to Doppler boosting. For less luminous objects, the disk-corona component accounts for a considerable fraction of the total X-rays, but it is by no means the dominant component, except for PG 0007+106. The latter is also consistent with the finding above that the X-ray continua are most likely not the same as, but flatter than that for radio-quiet quasars, which have $\Gamma \sim 2.0$ (Reeves & Turner 2000).

The highest fraction is in PG 0007+106, where the disk-corona X-ray emission dominates the total observed X-rays. It is expected to give its rather weak radio core emission and, thus, weak X-rays from the jet; the dominance of the disk-corona emission is also consistent with its relatively steep photon index ($\Gamma = 1.71 \pm 0.04$) of the underlying continuum, and with the prominent Fe Kα emission line in the XMM-Newton spectrum. The self-consistent result obtained for PG 0007+106 also implies that the above estimation of the disk-corona X-ray emission is reliable. For the remaining objects, adding a disk-corona component in the XMM-Newton spectra is consistent with the data, but does not improve the fits statistically, owing to their small fractions, i.e., this component cannot be constrained meaningfully in the spectral fits. It should be noted that, though the errors for individual objects are large, the result should be meaningful in the statistical sense.

5.2 Enhanced X-Ray Emission in Lobe-Dominated Objects

Since we have an estimate of the X-ray flux from the disk-corona component (under the assumption that the disk-corona X-ray–optical relation is the same for radio-loud and radio-quiet quasars), we can now examine whether this component is responsible for the X-ray emission seen in non-core-dominated objects (Fig. 6). We subtract the estimated luminosity of the disk-corona component from the observed total X-ray luminosity, and plot the leftover luminosity versus the radio core luminosity L_{rc} again in Figure 8. The X-ray and radio core-jet luminosity relation as given by Equation (1) is also indicated as in Figure 6. Compared to Figure 6, the X-ray luminosities have been shifted downward for all the objects. For core-dominated quasars the leftover X-rays are now even better consistent with the prediction of Equation (1), indicating that they come predominantly from jets in these objects. This is in agreement with X-ray unification schemes.

However, this is not the case for the lobe-dominated quasars. As revealed clearly in Figure 8, all of the four lobe-dominated quasars have the leftover X-ray luminosities systematically higher than the

predicted core-jet X-ray luminosity, by roughly one order of magnitude. The situation for mildly lobe-dominated quasars is between the lobe-dominated and core-dominated objects, which have relatively higher X-ray luminosities than expected but the deviations are relatively small, compared to lobe-dominated ones. Compared with Figure 7, it can be seen that in most of the objects this leftover X-ray emission is in fact the dominating or at least of the largest portion of the observed X-ray flux. We also examine the $L_x - L_c$ relation by using different L_x values. First, we simply take the fitted flat (underlying) continuum as L_x (i.e. no subtraction of the disk-corona component except the soft X-ray excess); second, we use the fitted flat component and subtract the above disk-corona contribution from it. We find that the results as shown in Figure 8 remain unchanged.

As a further examination of the above result, we investigate the $L_x - L_c$ relation at a higher energy, say, 10 keV, in order to eliminate the uncertainty introduced in estimating the disk-corona X-ray emission, which becomes weaker at higher energies for its relatively steep spectrum. At 10 keV, the contribution from the soft X-ray excess, if any, is negligible, and the total X-ray flux density is nearly the same as that of the flat component. We repeat the procedure as above, but using X-ray fluxes at 10 keV. For the disk-corona component, the 10 keV flux is extrapolated from the 2 keV assuming the canonical $\Gamma = 2.0$. The result is shown in Figure 9. Equation (1) from Brinkmann et al. (1997) is then converted to 10 keV (assuming $\Gamma = 1.6$ for jet X-ray emission) and is indicated as the solid line. This yields the same result as above, i.e., there exists excess X-ray emission in lobe-dominated quasars above the prediction from the simple core-jet radio–X-ray correlation.

We suggest that the systematically higher leftover X-ray fluxes than the predicted jet emission are most likely not an artifact due to, e.g. the systematics in estimating X-ray flux of the disk-corona component from the optical data between radio-loud and radio-quiet quasars. This is simply because, first, the luminosities of the leftover emission are actually much higher (by several times on average) than that of the disk-corona component. Second, the fact that in PG0007+106, where the disk-corona X-ray emission is expected to be dominant, the predicted X-ray luminosity matches well the observations.

### 5.3 Origin of Enhanced X-Ray Emission in Lobe-Dominated Objects

5.3.1 General discussion

If the above assumption is valid that the disk-corona UV/optical–X-ray luminosity relation for radio-quiet quasars can be used for radio-loud objects, the disk-corona X-rays, as estimated from the UV/optical luminosity, can account for only a small fraction of this additional X-ray emission for most of the objects. Some leftover X-ray flux remains systematically unaccounted for, which is about one order of magnitude higher than the prediction of the simple radio and X-ray core-jet luminosity relation.

Alternatively, if the above assumption is invalid, the observed X-rays may be explained as originating from disk-corona emission. In this case, radio-loud quasars should follow a different disk-corona X-ray–UV/optical luminosity relation as compared with radio-quiet objects in two aspects. First, a significantly higher X-ray luminosity is expected for radio-loud quasars than radio-quiet ones at the same UV/optical luminosity. Second, the spectral shape of this X-ray emission is flat, with $\Gamma \simeq 1.5$, significantly flatter than that for radio-quiet objects; either the X-ray spectra are intrinsically flat, or there exists substantial X-ray absorption in these quasars.

We conclude that in either case, there exists enhanced X-ray emission in lobe-dominated objects, regardless of its origin. In view of the largely similar accretion processes believed to be operating in radio-quiet and radio-loud quasars, and the flat spectral shape of this enhanced emission compared with that in radio-quiet quasars, we prefer to consider the first scenario to be more likely, though the disk-corona origin cannot be ruled out.

As a natural explanation, we hypothesize that this enhanced X-ray emission is from the X-ray jet. In other words we still see a substantial amount of jet X-ray emission even at a large jet inclination angle. If this is the case, it means that the X-ray and radio core-jet luminosity relation should flatten toward low radio core luminosity, rather than the simple relation as given by Equation (1). This is possible, since Equation (1) was established based on only core-dominated quasars (Brinkmann et al. 1997), which have mostly high radio core luminosities; the relation was actually extrapolated down to the low L_{rc} range in the simple unification schemes, as an assumption. The physical justification for this simple relation as in Equation (1) is that the X-ray and radio emission from jets must experience the same magnification factors due to the
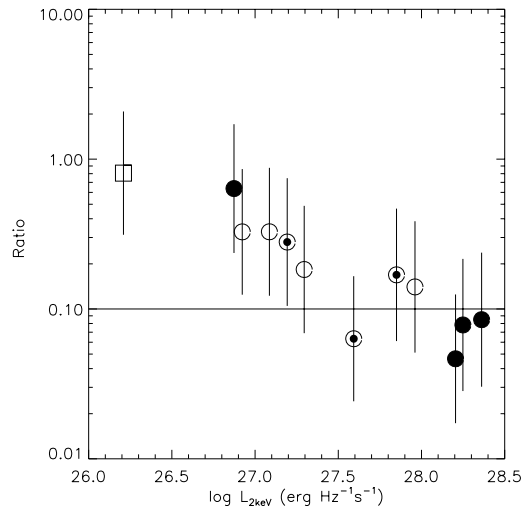
Fig. 7 Ratio of the luminosity of the disk-corona X-ray emission, estimated from the optical/UV continuum, to the observed total X-ray luminosity at 2 keV. The error bars represent the systematic uncertainty (1-σ) of the estimated disk-corona X-ray luminosity given by Shen et al. (2006), the solid line denotes a level of 10% of the observed X-ray luminosity. The symbols are the same as in Fig. 6.
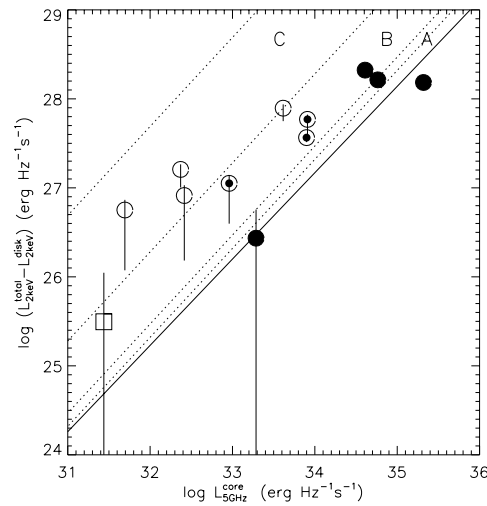
Fig. 8 Leftover X-ray luminosities at 2 keV, obtained by subtracting the contribution of the expected disk-corona component from the observed X-ray luminosity, are plotted against the radio core luminosity at 5 GHz. The error bars represent the systematic uncertainty (1-σ) of the estimated disk-corona X-ray luminosity given by Shen et al. (2006). The symbols and plotted lines are the same as in Fig. 6. The dotted lines represent the modeled relations for different jet inclination angles (core-dominance) from core-dominated to lobe-dominated quasars (from $0°$, $10°$, $15°$, $45°$ from bottom to top; zones A, B, and C correspond to the zones in Fig. 10), using the wide X-ray jet model proposed by Celotti et al. (1993, see Sect. 5.2 for details). For PG 0007+106, the predicted disk emission is statistically consistent with the observed total X-ray luminosity, and the leftover luminosity not significantly detected is consistent with zero and represented by error bars only. See Sects. 4.3 and 5.2 for details.
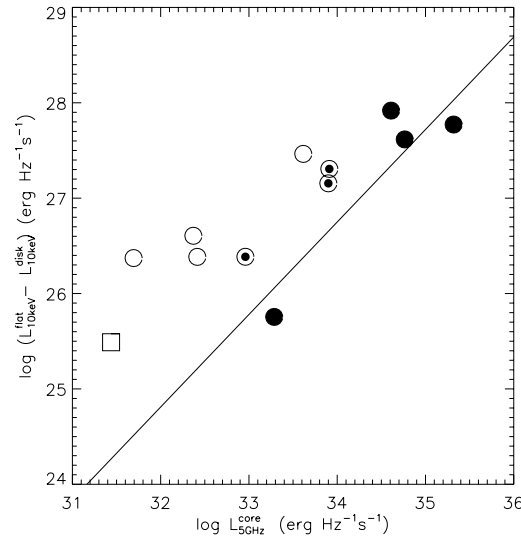
Fig. 9 Leftover X-ray luminosities at 10 keV, obtained by subtracting the contribution of expected disk-corona component from the observed X-ray luminosity plotted against the radio core luminosity at 5 GHz. The symbols and plotted lines are the same as in Fig. 6.

Doppler boosting effect, when viewed at a given inclination angle. However, in reality this may not be the case. If the X-ray jet emission is less Doppler beamed than the radio jet, the $L_x - L_{rc}$ relation will become flattened at low L_{rc} (c.f. that in Fig. 8) with an increasing inclination angle of the jet axis to the line of sight, and this may explain our observational results qualitatively. Since extensive exploration of the underlying physical mechanism responsible for such a condition is beyond the scope of this paper, we would like just to check one possibility below as a plausible explanation of our results, namely, the wide X-ray jet model, in which the X-ray and radio jets have different opening angles.

5.3.2 A plausible explanation – a wide X-ray jet model

As for a model that the X-ray jet subtends an opening angle larger than that of the radio jet, we understand it is not the unique explanation, but just a plausible one. We defer to a future study for further explorations of various models, which may better explain the result found in this paper.

Such a wide X-ray jet model has been proposed by Celotti et al. (1993), in an attempt to unify X-ray and radio selected BL Lac objects, and has been invoked to explain some observed properties of blazars (Lenain et al. 2008; Hardcastle et al. 2003; Rector et al. 2003). A relativistic flow is considered with a constant bulk Lorentz factor γ but with velocity vectors uniformly spread in a cone of semi-aperture Θ_j, which is larger than the critical semi-aperture angle for relativistic beaming Θ_c, where $\sin\Theta_c = 1/\gamma$. The X-ray emitting jet has Θ_j larger than the radio emitting jet, and hence a much weaker relativistic beaming effect than the latter does. At a given inclination angle Θ with the jet axis, the observed luminosity $L(\Theta)$ is linked to the intrinsic luminosity l via
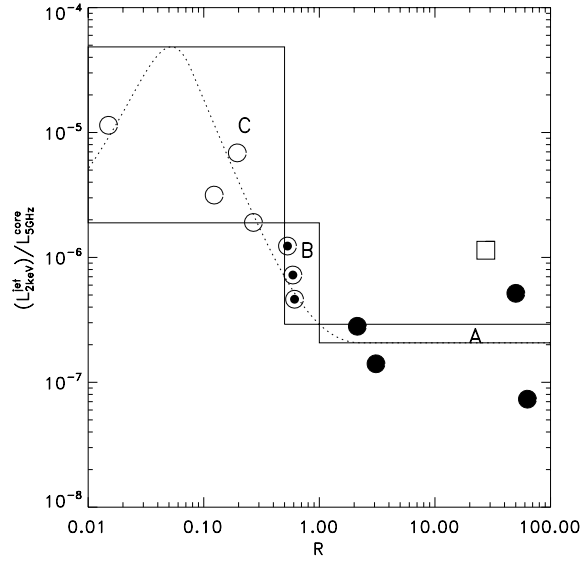
$$L(\Theta) = lR(\Theta), \tag{3}$$

where $R(\Theta)$ is the Doppler enhancement factor. Celotti et al. (1993) gave approximation calculations for $R(\Theta)$ in two regimes of $R(\Theta)$ ($\Theta < \Theta_j$ and $\Theta > \Theta_j$) as

$$R(\Theta) = \frac{2\pi}{\Delta\Omega_j}(1+\beta)^{p-1}\gamma^{p-2}, \quad \Theta < \Theta_j, \tag{4}$$

and

$$R(\Theta) = \frac{2\pi}{\Delta\Omega_j}\frac{1}{(1+\beta)\gamma^{p+2}[1-\beta\cos(\Theta-\Theta_j)]}, \quad \Theta > \Theta_j, \tag{5}$$

Fig. 10 X-ray to radio luminosity ratio of emission from jets versus core-dominance R predicted from the wide-jet model (see text). The three zones, A, B and C, denote the upper- and lower-bounds of the same flux ratios predicted from the wide X-ray jet model for core-dominated, mildly lobe-dominated and lobe-dominated quasars, respectively. The dotted curve represents a predicted dependence of the luminosity ratio on R by the model adopting a specific relation for R and the jet inclination angle. Plotted are the observed luminosity ratio between the leftover X-ray (obtained by subtracting the contribution of the expected disk-corona component from the observed X-ray luminosity at 2 keV) and the radio core at 5 GHz for our objects. The symbols are the same as in Fig. 6. PG 0007+106 is not plotted since there is no significant leftover emission detectable from it.

where $\Delta\Omega_{\mathrm{j}} = 2\pi(1 - \cos\Theta_{\mathrm{j}})$ and $\beta = \sqrt{1 - (1/\gamma)^2}$. We assume the following jet parameters typical of radio-loud quasars, $\Gamma = 10$, $p = 3$ for a moving sphere, the semi-aperture angle $\Theta_{\mathrm{jr}} = 8°$ for the radio jet, and $\Theta_{\mathrm{jx}} = 20°$ for the X-ray jet. For a given set of jet parameters, the radiation enhancement factor $R(\Theta)$ can be computed for a given inclination angle Θ.

For a direct comparison with the observations, we calculate the ratio between the enhancement factors of the X-ray and the radio jet, which can be linked to the observed X-ray to radio jet luminosity ratio,

$$\frac{L_{\mathrm{x}}(\Theta)}{L_{\mathrm{r}}(\Theta)} = \frac{R_{\mathrm{x}}(\Theta)}{R_{\mathrm{r}}(\Theta)} \frac{l_{\mathrm{x}}}{l_{\mathrm{r}}}, \tag{6}$$

where $l_{\mathrm{x}}/l_{\mathrm{r}}$ is the intrinsic luminosity ratio, assumed to be constant and treated as a free parameter. An X-ray to radio jet luminosity ratio $L_{\mathrm{x}}(\Theta)/L_{\mathrm{r}}(\Theta)$ can be predicted from the model for a given inclination angle Θ, and for an assumed $l_{\mathrm{x}}/l_{\mathrm{r}}$.

However, one difficulty is the lack of measurement of the inclination angle Θ for our objects. The core-dominance parameter, as an indicator of Θ, cannot be related to Θ directly without involving specific models, but still, we can constrain the range of Θ using the core-dominance parameter, based on previous studies. It has been shown that in core-dominated quasars the inclination angles are less than $10°$, while in lobe-dominated quasars they are in the range of $10°$ and $40°$ (Ghisellini et al. 1993). We thus assume $\Theta = 0°-10°$ for the core-dominated ($R > 1$) objects, $\Theta = 10°-15°$ with $0.5 < R < 1$, and $\Theta = 15°-45°$ with $R < 0.5$ in our sample. The division of Θ between $0.5 < R < 1$ and $R < 0.5$ for different objects is somewhat arbitrary, but the exact number does not affect our result qualitatively. For each of the three core-dominance categories, we compute the upper- and lower-bounds of the X-ray to radio jet flux ratio, which correspond to the lower and upper limits of Θ, as shown in Figure 10 (zones A, B and C).

We compare the data with the model in Figure 10, in which the ratio between the leftover X-ray luminosity (obtained by subtracting the contribution of the expected disk-corona component from the observed

total X-ray flux at 2 keV) and the 5 GHz radio core-jet luminosity is plotted as a function of core-dominance. PG 0007+106 is not plotted since no significant leftover emission has been detected from it. It can be seen that the observed luminosity ratios fall mostly within the predicted zones from such a model and this is especially true for non-core-dominated objects (zones B and C). With the decrease of R from moderate to low values, the observed luminosity ratio of X-ray to radio core emission from jet increases dramatically, by up to 1–2 orders of magnitude. This then naturally explains the excess X-ray emission with flat X-ray spectrum seen in non-core-dominated quasars in our result. Among the two core-dominated objects showing large scatters, the deviations might be caused by a different intrinsic luminosity ratio between the two bands, $l_{\rm x}/l_{\rm r}$, or simply by flux variations which are typical of jet X-ray emissions in core-dominated quasars. The modeled X-ray to radio core-jet luminosity ratios can be plotted back in Figure 8 as dotted lines, which correspond to the range of the jet viewing angle for the three categories (the upper and lower bounds of the zones A, B and C in Fig. 10). These modeled lines explain naturally the flattened $L_{\rm x} - L_{\rm rc}$ relation for lobe-dominated quasars (with larger jet viewing angle Θ), compared to the relation for core-dominated quasars (small Θ values). Thus the observed $L_{\rm x} - L_{\rm rc}$ relation in our sample can be explained.

To give an insight into the modeled relation of the jet X-ray to the radio luminosity ratio with R, we adopt a specific, though somewhat arbitrarily chosen relation between R and Θ[5], and show the modeled relation in Figure 10 (dotted line). We conclude that a wide X-ray jet model, as proposed by Celotti et al. (1993), can well explain the observed excess X-ray emission seen in lobe-dominated quasars. We note that the above results are insensitive to the choice of the model parameters, which can be accommodated in a large volume of the parameter space. This is also true for $p = 2$ (appropriate for a continuous jet).

6 SUMMARY

We study the orientation dependent X-ray properties of radio-loud quasars by using a sample of 12 objects observed with XMM-Newton, which covers a wide range of the radio core-dominance parameter, R, from core-dominated to lobe-dominated objects. We analyze the X-ray spectroscopic data, and for most of which the results are presented for the first time. We find that, for the core-dominated sources, a single flat power-law (average $\Gamma \sim 1.5$) can well describe the X-ray spectra in some objects, while an extra soft X-ray component is needed on top of that in the others. For the lobe-dominated quasars, X-ray spectra are best fitted with also a *flat* underlying power-law (average $\Gamma \sim 1.6$) plus a soft X-ray excess. Similar results are found for mildly lobe-dominated objects. The flat spectral shape of the underlying continuum found for all but one of the objects of these two types (non-core-dominated) is somewhat surprising. In fact, the photon indices of the underlying continuum are indistinguishable among the three R categories. This is well consistent with the previous knowledge for core-dominated quasars, whose X-ray emission is predominately from the jets and significantly boosted due to relativistic beaming. This result is at odds with what was generally thought previously for lobe-dominated quasars. A similar result was also found recently by Belsole et al. (2006).

We confirm that the X-ray luminosity is correlated with the radio core luminosity, but with a slope much flatter than that derived on the basis of core-dominated quasars only and extrapolated to low-R objects. This means that, in low-R quasars, where the observed radio-core emission is generally weak, the X-ray emission is much stronger than the expected jet emission from the simple X-ray and radio core-jet luminosity relation commonly assumed. This is in line with previous findings.

We examine whether this extra X-ray emission can be explained by the disk-corona X-rays produced in the black hole accretion process. Our method is to estimate its contribution from the optical/UV continuum assuming that radio-loud quasars follow the same X-ray–UV/optical luminosity relation for disk-corona emission found for radio-quiet quasars. We find that, however, neither the luminosity nor the spectral shape of the disk-corona X-ray emission can account for the bulk of the observed X-rays, which is in excess of the predicted jet emission from previous simple unification models by one order of magnitude or more. We are left with two options in explaining the X-rays from lobe-dominated quasars: either the disk-corona X-ray emission is much enhanced in strength and flatter in spectral shape ($\Gamma \sim 1.5$) compared to normal radio-quiet quasars, or their jet X-ray emission is much enhanced. We argue that the latter is likely the case, though the former cannot be ruled out. This is most likely due to the different Doppler beaming effect for the

---

[5] The modeled $L_{\rm x}(\Theta)/L_{\rm r}(\Theta) - \Theta$ relation is insensitive to the exact function form chosen for the $R - \Theta$ relation.

radio and the X-ray emission, with the latter less beamed than the former, though the underlying physical reason is unknown. As an example, we consider a specific model which can lead to such a condition, in which the X-ray emitting jet has a larger opening angle than the radio jet, as proposed by Celotti et al. (1993).

References

Baker J.C., Hunstead R.W., Brinkmann W., 1995, MNRAS, 277, 553

Belsole E., Worrall D. M., Hardcastle M. J., 2006, MNRAS, 366, 339

Brinkmann W., Yuan W., Siebert J., 1997, A&A, 319, 413

Brinkmann W., Otani C., Wagner S. J., Siebert J., 1998, A&A, 330, 67

Browne I. W. A., Murphy D. W., 1987, MNRAS, 226, 601

Brunetti G., Cappi M., Setti G., Feretti L., Harris D. E., 2001, A&A, 372, 755

Brunetti G., Bondi M., Comastri A., Setti G., 2002 A&A, 381, 795

Brunetti G., Setti G., Comastri A., 1997, A&A, 325, 898

Celotti A., Maraschi L., Ghisellini G., Caccianiga A., Maccacaro T., 1993, ApJ, 416, 118

Dickey J., Lockman F. J., 1990, ARA&A, 28, 215

Elvis M., Lockman F., Wilkes B. J., 1989, AJ, 97, 777

Falcke H., Patnaik A. R., Sherwood W., 1996, ApJ, 473, 13

Fanaroff B. L., Riley J. M., 1974, MNRAS, 167, 31

Fiore F., Elvis M., Giommi P., Padovani P., 1998, ApJ, 492, 79

Gambill J. K., Sambruna R. M., Chartas G. et al., 2003, A&A, 401, 505

Ghisellini G., Padovani P., Celotti A., Maraschi L., 1993, ApJ, 407, 65

Gliozzi M., Sambruna R. M., Brandt W. N., 2003, A&A, 408, 949

Hardcastle M. J., Birkinshaw M., Cameron R. A. et al., 2002, ApJ, 586, 123

Hardcastle M. J., Worrall D. M., Birkinshaw M., Canosa C. M., 2003, MNRAS, 338, 176

Harris D.E., Grindlay J. E., 1979, MNRAS, 309, 969

Haves P., Conway R. G., Stannard D., 1974, MNRAS, 1974, 169, 117

Hutsemékers D., Cabanac R., Lamy H., Sluse D., 2005, A&A, 441, 915

Isobe N., Tashiro M., Makishima K. et al., 2002, ApJ, 580, L111

Isobe N., Makishima K., Tashiro M., Hong S., 2005, ApJ, 632, 781

Ivezić Ž. et al. 2002, AJ, 124, 2364

Jansen F., Lumb D., Altieri B. et al., 2001, A&A, 365, L1

Jiménez-Bailón E., Piconcelli E., Guainazzi M. et al., 2005, A&A, 435, 449

Kalberla P. M. W., Burton W. B., Hartmann D. et al., 2005, A&A, 440, 775

Kataoka J., Leahy J. P., Edwards P. G. et al., 2003, A&A, 410, 833

Kataoka J., Stawarz L., 2005, ApJ, 622, 797

Kellermann K. I., Sramek R., Schmidt M., Shaffer D. B., Green R., 1989, AJ, 98, 1195

Kembhavi A., Feigelson E. D., Singh K. P., 1986, MNRAS, 220, 51

Kembhavi A., 1993, MNRAS, 264, 683

Kirsch M. et al., 2007, 'EPIC status of calibration and data analysis', 2007, XMM-Newton SOC, XMM-SOC-CAL-TN-0018 (August, 13, 2007)

Kovalev Y. Y., Kellermann K. I., Lister M. L. et al., 2005, AJ, 130, 2473

Kraft R. P., Birkinshaw M., Hardcastle M. J. et al., 2007, ApJ, 659, 1008

Landt H., Perlman E. S., Padovani P. 2006, ApJ, 637, 183

Lawson A., Turner M. J. L., 1997, MNRAS, 288, 920

Lenain J.-P., Boisson C., Sol H., Katarzyński K., 2008, A&A, 478, 111

Lister M. L., Homan D. C., 2005, AJ, 130, 1389

Loiseau N. et al., 2005, "User's Guide to the XMM-Newton Science Analysis System v.3.2", European Space Agency - XMM-Newton Science Operations Centre (*http://xmm.vilspa.esa.es/sas/*)

Nandra K., George I. M., Mushotzky R. F., TUrner T. J., Yaqoob T., 1997a, ApJ, 488, L91

Nandra K., George I. M., Mushotzky R. F., TUrner T. J., Yaqoob T., 1997b, ApJ, 477, 602

Orr M., Browne I., 1982, MNRAS, 200, 1067

Piconcelli E., Jiménez-Bailón E., Guainazzi M. et al., 2005, A&A, 432, 15

Rector T. A., Gabuzda D. C., Stocke J. T., 2003, AJ, 125, 1060

Reeves J. N., Turner M. J. L., 2000, MNRAS, 316, 234

Salvi N. J., Page M. J., Stevens J. A. et al., 2002, MNRAS, 335, 177

Shastri P., 1991, MNRAS, 249, 640

Shen S., White S. D. M., Mo H. J. et al., 2006, MNRAS, 369, 1639

Siebert J., Brinkmann W., Drinkwater M. J. et al., 1998, MNRAS, 301, 261

Siemiginowska A., Stanghellini C., Brunetti G. et al., 2003, ApJ 595, 643

Sitko M. L., Zhu Y., 1991, ApJ, 369, 106

Stark A. A., Gammie C. F., Wilson R. W., 1992, ApJS, 79, 77

Stockton A., Fu H., Henry J. et al., 2006, ApJ, 638, 635

Tananbaum H., Wardle J. F. C., Zamorani G., Avni Y., 1983, ApJ, 268, 60

Teräsranta H., Wiren S., Koivisto P. et al., 2005, A&A, 440, 409

Urry C. M., Padovani P., 1995, PASP, 107, 803

Veron-Cetty M.-P., Veron P., 1993, A Catalogue of Quasars and Active Nuclei, 6th ed., ESO Scientific Report No. 13

Wilkes B. J., Elvis M., 1987, ApJ, 323, 243

Williams O. R., Turner M. J. L., Stewart G. C. et al., 1992, ApJ, 389, 157

Yuan W., Brinkmann W., Siebert J., Voges V., 1998, A&A, 330, 108

Yuan W., Brinkmann W., Gliozzi M., Zhao Y., Matsuoka M., 2000, A&A, 362, 19

Yuan W., Fabian A. C., Celotti A., Jonker P. G., 2003, MNRAS, 346, L7